



Efficient modeling of phase change material solidification with multidimensional fins



Chunjian Pan^{a,*}, Sean Hoenig^b, Chien-Hua Chen^b, Sudhakar Neti^a, Carlos Romero^a, Natasha Vermaak^a

^a Lehigh University, Bethlehem, PA 18015, USA

^b Advanced Cooling Technologies, Inc., Lancaster, PA 17601, USA

ARTICLE INFO

Article history:

Received 25 June 2017

Received in revised form 25 July 2017

Accepted 26 July 2017

Keywords:

Latent energy storage
Efficient PCM modeling
PCM with internal fins
Optimal fin design

ABSTRACT

Phase Change Materials (PCMs) are gaining importance in energy storage applications. Many PCM are poor thermal conductors and thus can gain from the optimal use of appropriate fins. Phase change process is inherently nonlinear in behavior due to the latent heat, thus simulations are usually based on finite difference or finite element approaches, which can be computationally inefficient for optimal design of latent energy storage systems. A novel modeling approach called Layered Thermal Resistance (LTR) model is proposed for the first time in this paper for efficient PCM simulations in multi-dimensions. The LTR model can be coupled with multidimensional fins for PCM-fin structure optimal design. Compared with CFD results, the results by the LTR model are high accurate in estimating the solidification time and the highlight is it has negligible simulation cost. Moreover, accurate heat flux of a finned PCM system is also obtained. The LTR model represents the nonlinear solidification process in a finned latent energy storage structure with analytic equations, thus it has bright applications in PCM heat sink optimization with internal fins.

© 2017 Elsevier Ltd. All rights reserved.

1. Introduction

Abundant research has been devoted to thermal energy storage systems due to their important role in clean energy technologies and matching renewable energy to load patterns. A good example is the mismatch between supply and demand of solar energy and thermal energy storage systems can play a major role. ‘Cold storage’ produced at a lower costs during off peak hours of the day is a practical way to release utilities’ burden to produce enough electricity during high demand hours [1,2].

Many mature and industrial applications of thermal energy storage systems use sensible energy. Phase Change Materials (PCMs) are receiving more attention due to their high-energy densities. PCM can store or release energy at near isothermal conditions that are thermodynamically superior [3]. The thermal reliability and stability of the PCMs was reviewed by Rathod [4]. However, the low conductivity of PCM materials is a barrier for many practical applications [3], especially for large scale systems. Researchers are eager to resolve this issue by analyzing different heat transfer enhancement techniques, i.e., including high conductivity foams or metal matrices into the PCM [5], dispersing high conductivity particles in the PCM [6], or use microencapsulation of the PCM [7]. Work conducted by Lohrasbi [8,9] indicated that

immersing innovative fin structures into PCM as a heat transfer enhancement technique is superior to nanoparticles dispersion. Plenty of research has been conducted to study the PCM system with fin structures since they can be simple and compact [10–12]. Sheikholeslami and Lohrasbi [13–15] studied the Nano-particle Enhanced PCM (NEPCM) and innovative fin structures in a combined way to increase the performance of the latent heat thermal energy storage system (LHTESS). Corrosion between PCM ($\text{CaCl}_2 \cdot 6\text{H}_2\text{O}$) and fin was recently reported by Ren [16].

Mathematical modeling plays important role for analyzing the performance of energy storage systems with PCMs. Henry [17] reviewed major methods of mathematical modeling of solidification and melting. An elegant Neumann’ solution is available for a one-dimensional semi-infinite region with simple initial and boundary conditions and constant thermal properties, as first presented by Stefan [18]. Many real world solidification problems are rarely one dimensional, and usually have complex initial and boundary conditions. Thus computational fluid dynamics (CFD) is widely employed in modeling PCMs. However, CFD is not always the efficient tool for optimal design of a LHTESS. Optimizations have been often based on parametric studies through simulations [10]. Multiple simulations need to be carried out for variations of the design parameters of interest. More efficient modeling with high accuracy and smaller CPU time as discussed here can be immensely beneficial to the design and optimization of a LHTESS.

* Corresponding author.

E-mail address: chp313@lehigh.edu (C. Pan).

Nomenclature

T_m	the exact PCM solidification temperature	$\Delta v_l(i)$	volume of each discrete layer for the 2-D and 3-D cases
T_w	cooling temperature at the boundary	T_{upper}	upper PCM melting temperature
t_{Neu}	PCM solidification time for Neumann's solution	T_{lower}	lower PCM melting temperature
t_{LTR}	PCM solidification time estimated by the LTR model	H, H_{ref}	specific PCM enthalpy and a referenced enthalpy value
t_{CFD}	PCM solidification time estimated by the CFD model	T_{cell}	temperature of a discrete element
ε	percent error	ΔT	driving temperature difference
s	distance of solidification front	φ	liquid fraction of PCM
Δs	thickness of each discrete layer for a 1-D PCM bar	x, y, z	locations of solidification fronts in x, y, z directions
N	number of discrete PCM layers	a, b, c	side lengths of a cuboid
A	cross section area of a 1-D PCM bar	μ, γ	side length ratios of a rectangle or a cuboid
ΔV	volume of each discrete layer for a 1-D PCM bar	α	resistance tuning factor value
q	heat flux	δ	thickness of fin
$R(i), R_f(i), R_{ij}(i)$	thermal resistances for heat transfer to the PCM layer i	h	heat transfer coefficient in the PCM side
$t(i)$	discrete solidification time for PCM layer i	L	distance from the fin to the solidification front of PCM
t_s	total solidification time	k_{fin}	conductivity of the fin
R_t	total thermal resistance of a system	l	length of a 1-D fin
L_m	latent energy of PCM	η	fin efficiency
Cp_{pcm}	heat capacity of PCM	ξ	parameter for fin efficiency calculation
k_{pcm}	conductivity of PCM	$\psi(0)$	dimensionless superheating parameter
ρ_{pcm}	density of PCM	T_{ini}	initial temperature of the PCM domain

Though many finite difference or finite element based methodologies have been developed for modeling PCM and PCM with heat transfer enhancement techniques, very few simple and efficient modeling techniques for simulation of PCM are in vogue. Efficient modeling of PCM freezing thus has room for improvement and useful applications. An approximate analytical model is presented to model the solidification and solidification of a finned PCM in one and two dimensions [19–21]. A fast 1-D analytical model is proposed in [22] to simulate the behavior of a wallboard containing the PCM and good prediction is achieved compared with CFD results. In this paper an efficient modeling approach called Layered Thermal Resistance (LTR) model is proposed for the first time to model the solidification process that is applicable for 2-D and 3-D geometries with fins. The highlight of the method is its ease with which it can include extended fins. That enables the method to be efficient and useful in optimization and design of a LHTESS with fins. The model is conduction based, so it is suitable for the energy discharging process, as many studies have demonstrated that during solidification natural convection exits only in the very beginning and soon conduction dominates the whole process [23]. For many processes involving energy charging and discharging, the freezing is often the resistance dominated process, thus posing a harder design goal to achieve, i.e., solidify the PCM within required time period. So an efficient coupled PCM-fin modeling method has useful applications for optimal design during the freezing process when fins are to be used.

The content of this paper is organized as follows. In Section 2, the efficient PCM modeling approach called Layered Solidification Front model shorthand noted as LTR model is described in 1-D, 2-D and 3-D and its performance is compared with CFD results. In Section 3, the construction of LTR models coupled with fins is given in 2-D and 3-D and their performance were tested against the CFD results. Section 4 summaries the efficient PCM modeling technique and suggests further study to develop and improve the method.

2. Layered thermal resistance model for PCM solidification

This section introduces the construction of the Layered Thermal Resistance (LTR) models for PCM solidification in multiple dimensions including 1-D, 2-D and 3-D.

2.1. 1-D layered solidification front model for fast PCM modeling

In this section the novel approach for efficient PCM solidification modeling in 1-D is developed and its results were compared to the Neumann's solution. The idea for the proposed LTR model is assuming that the liquid PCM is solidified layer by layer and the final solidification time is estimated by adding together the solidification times of all the discrete layers.

A 1-D semi-infinite PCM bar is shown in Fig. 1. Assuming its exact solidification temperature is T_m , cooled by constant Temperature T_w at one end and has zero flux for the remaining sides. The initial temperature of the bar everywhere is assumed to be T_m . It should be noted that when the initial temperature equals to the solidification temperature, there is no heat loss at the solidification interface for a semi-infinite bar, so the solidified distance given by the Neumann's solution is equivalent to a fixed bar. Thus given certain solidification time t_{Neu} , the solidification front s can be estimated by Neumann's solution [17]. Then the LTR model is applied to the solidification front s to estimate its solidification time t_{LTR} . The performance of the LTR model is evaluated by comparing the estimated solidification time to that was assigned to the Neumann's solution. Estimation accuracy in terms of percent error is defined as

$$\varepsilon = \frac{(t_{LTR} - t_{Neu})}{t_{Neu}} \times 100\%. \quad (2.1)$$

To implement the LTR model, the solidification front s is equally divided into $N - 1$ pieces, called layered solidification fronts. The volume for each piece is ΔV . The distance between the solidification front and cooling surface determines the thermal resistance to pass energy into the current layer, thus prescribing the magnitude of heat flux going into the layer. The solidification time for

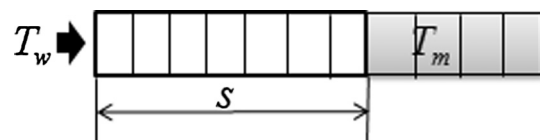


Fig. 1. 1-D PCM bar.

each of the discrete layer is then determined through dividing the total energy in the discrete layer by its current heat flux. The final solidification time is estimated by adding those solidification times of all the discrete layers. Eqs. (2.2)–(2.7) shows this process in 1-D. The heat flux (2.5) is also obtained for the entire solidification process.

$$\Delta s = \frac{s}{N - 1} \tag{2.2}$$

$$\Delta V = \Delta s A \tag{2.3}$$

$$R(i) = \frac{i \Delta s}{A k_{pcm}} \tag{2.4}$$

$$q(i) = \frac{T_m - T_w}{R(i)} \tag{2.5}$$

$$t(i) = \frac{\Delta V \rho_{pcm} [L_m + 0.5 C p_{pcm} (T_w - T_m)]}{R_t(i)} \tag{2.6}$$

$$t_s = \sum_{i=1}^{N-1} t(i). \tag{2.7}$$

Given certain PCM properties which are used throughout this paper (see Table 1), different solidification times t_{Neu} and driving temperature difference $dT = T_m - T_w = 10^\circ\text{C}$, the Neumann's solution [17] gives the distances of the solidification fronts. The LTR model was used to estimate the solidification time to reach those fronts. Table 2 shows that the LTR model has high accuracy. However, there is some constant overestimated error based on the LTR model. This means there is some small default error within the model itself. The most possible source for this constant deviation is that the average temperature difference $0.5(T_m - T_w)$ is used to account for the sensible energy in Eq. (2.6) for each of the discretized layer, and it may overestimate the sensible energy compared with Neumann's solution. Grids sensitivity analysis is given in Table 3. $t_{Neu} = 10$ h is the target solidification time to be achieved by the LTR model. Table 3 shows that more discrete layers will increase the accuracy of the LTR model, while insufficient number of layers will lead to large deviations.

2.2. LTR model for 2-D

This section introduces the LTR model to 2-D PCM solidification modeling with constant cooling temperature at boundaries. Extra tuning parameter has to be introduced to successfully apply the LTR model in 2-D. Fig. 2 shows the layered solidification fronts in a rectangle. It is cooled on the two sides with constant temperature, and has zero heat flux at the other two sides. The modeling approach is shown in Eqs. (2.8)–(2.13), where a is the thickness of the domain out of the paper. Variables x and y denote the locations of the freezing front. Two heat paths with the two thermal resistances R_1 and R_2 are regarded to transfer heat to the freezing front. And average temperature difference $0.5(T_m - T_w)$ is used to account for the sensible energy.

$$R_1(i) = \frac{x(i)}{a(c - y(i))k_{pcm}} \tag{2.8}$$

$$R_2(i) = \frac{y(i)}{a(b - x(i))k_{pcm}} \tag{2.9}$$

$$R_t(i) = \frac{R_1(i)R_2(i)}{R_1(i) + R_2(i)} \tag{2.10}$$

$$q(i) = \frac{T_w - T_m}{R_t(i)} \tag{2.11}$$

$$t(i) = \frac{\Delta V_1(i) \rho_{pcm} [L_m + 0.5 C p_{pcm} (T_w - T_m)]}{q(i)} \tag{2.12}$$

$$t_s = \sum_{i=1}^{N-1} t(i). \tag{2.13}$$

Computational Fluid Dynamics (CFD) simulation results are used to verify the LTR model. The Solidification & Melting Model [24] which is based on the enthalpy-porosity method [25] is implemented in Fluent (commercial CFD software) to obtain the numerical solutions. For the enthalpy-porosity method, three regions, solid, liquid, and mushy zones, are defined in the computational domain. Given a PCM's melting range (T_{lower}, T_{upper}) and a cell temperature T_{cell} , a liquid fraction ranging from 0 to 1 is defined by Eq. (2.14) and is used to identify the three regions.

$$\varphi = \begin{cases} 1, & T_{cell} > T_{upper} \\ \frac{T_{cell} - T_{lower}}{T_{upper} - T_{lower}}, & T_{lower} \leq T_{cell} \leq T_{upper} \\ 0, & T_{cell} < T_{lower} \end{cases} \tag{2.14}$$

As the solidification process is conduction dominated [18], the continuity and momentum equations were turned off in the Fluent setup. Thus energy balance is the main governing equation:

$$\frac{\partial}{\partial t} (\rho_{pcm} H) = \nabla \cdot (k_{pcm} \nabla T) \tag{2.15}$$

where specific enthalpy H is formulated according to enthalpy method [25].

$$H = H_{ref} + \int_{T_{ref}}^T C p_{pcm} dT + \varphi L_{pcm} \tag{2.16}$$

Validation of the solidification phenomenon by the enthalpy method [25] against the experimental data is available in Ismail's work [26]. Fig. 3 directly cited from [26] shows good comparison of solidification fronts between the numerical and experimental results. The $\psi(0)$ in the figure is a dimensionless superheating parameter defined as $\psi(0) = (T_{ini} - T_m) / (T_{ini} - T_w)$ to represent the system with different initial temperature, where T_{ini} is the initial temperature of the system. It should be noted that the exact solidification temperature to be used in the LTR model is defined as $T_m = \frac{1}{2}(T_{lower} + T_{upper})$.

For the simulations in this study, the total number of elements is 10,000–40,000 and the time step is 3–6 s depending on the size of the geometry. Sensitivity studies were performed to confirm mesh and time-step independence of the results presented. The energy equation was discretized using the Second Order Upwind scheme. A pressure based solver with double-precision was chosen. The convergence was checked at every 2 time steps with the scaled absolute residual of 10^{-9} was used for the energy equation.

Table 4 shows the rectangular PCM domain with different aspect ratios to be used to test the LTR model. The ratios here range from 0.025 to 1. It should be noted that an aspect ratio 0.025 can also represent the ratio 40. The CFD results were treated as trusted reference to validate the LTR model. From left plot in Fig. 4, it can be seen that the LTR model overestimates the solidification time

Table 1
Thermal properties of certain PCM used in this paper (for simplicity, the same properties are used for the solid and liquid phases).

Density	Conductivity	Heat capacity	Latent heat
1600 kg/m ³	0.5 W/(m K)	2000 J/(kg K)	120 kJ/kg

Table 2
Performance of the LTR model.

Given solidification time t_{Neu} (h)	1	3	5	7	10
Solidification front distances by Neumann's solution (cm)	1.33	2.31	2.98	3.53	4.22
t_{LTR} (h)	1.0285	3.085	5.142	7.199	10.285
ε	2.85%	2.85%	2.85%	2.85%	2.85%

Table 3
Effect of number of discrete layers on the accuracy of the LTR model.

Number of layers	9999	999	99	49	29	9	2
t_{LTR}	10.275	10.285	10.378	10.484	10.629	11.416	15.411
ε	2.75%	2.85%	3.78%	4.84%	6.29%	14.16%	54.12%

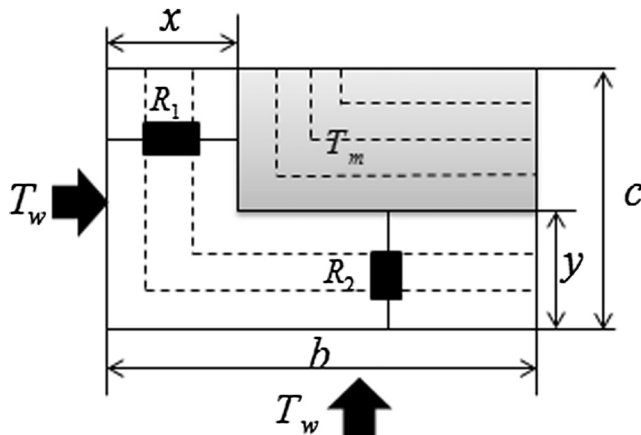


Fig. 2. Layered moving fronts for a rectangular PCM.

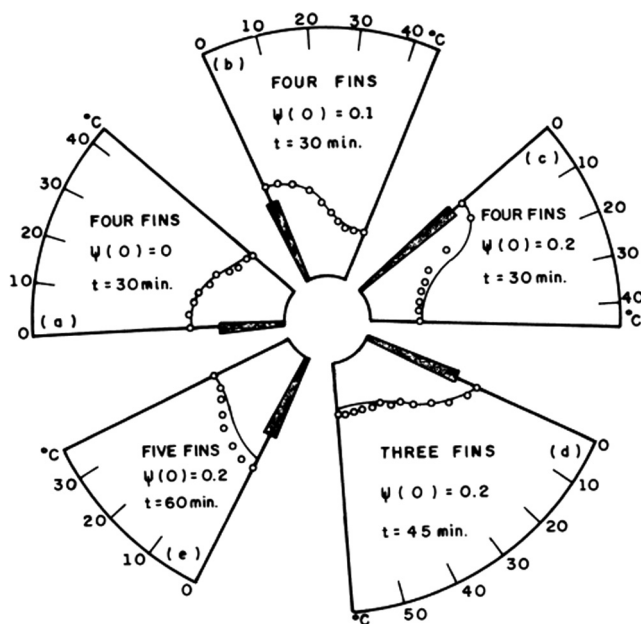


Fig. 3. Comparison of numerical and experimental solidification fronts [26].

for the 10 cases by around 50–60% compared with the CFD results. This means adjustment can be made to improve the accuracy of the LTR model. The right plot in Fig. 4 shows a nice curve can be fitted between the solidification time ratios t_{CFD}/t_{LTR} of the two models and the aspect ratios c/b of a rectangle. The solidification time ratio of the two models actually indicates how much thermal resistance was overestimated by the LTR model. From this perspective, the

ratio can be treated as a tuning parameter to adjust the total resistance in the LTR model. The LTR model modified with a tuning factor is then called the tuned LTR model in the following context.

A regression model was built by custom support vector regression (SVR) which is also available as MATLAB toolbox [27] to predict the resistance tuning factor for the LTR model. Other curve fitting techniques can also be employed such as simple linear fitting or spline interpolation [28]. Generally, SVR has more generalization ability with a small training sample [29] which means higher prediction accuracy than other methods. In Eqs. (2.17)–(2.19), the aspect ratio μ is the independent variable for the SVR model f_1 while α is the output resistance tuning parameter (solidification time ratio of the LTR and CFD models t_{LTR}/t_{CFD}), which is used to adjust the total resistance of the LTR model. The 7 cases' data is used to train and build the SVR model $\alpha = f_1(\mu)$. Fig. 5 shows the regression curve. It is the reconstruction curve of the solidification time ratio versus aspect ratio of a rectangle. What needed to be emphasized is that the aspect ratio is covered from 0.025 to 1, which can also represent a ratio range from 1 to 40, so this aspect ratio range includes a large number of rectangular shapes. When estimating the solidification time of a new rectangle PCM, its aspect ratio should fall within this range.

$$\alpha = f_1(\mu) \tag{2.17}$$

$$\mu = \frac{c}{b} \tag{2.18}$$

$$R_t(i) = \alpha \frac{R_1(i)R_2(i)}{R_1(i) + R_2(i)} \tag{2.19}$$

For the 7 cases simulated by the CFD method in Fluent, a solidification temperature range $T_{upper} - T_{lower} = 2^\circ\text{C}$ is set, the initial temperature is T_{upper} everywhere, $T_{upper} - T_w = 10^\circ\text{C}$ and the conductivity of the PCM is $k_{pcm} = 0.5 \text{ W/m K}$. In the LTR model the driving temperature difference $\Delta T = T_m - T_w = 9^\circ\text{C}$, as it is assumed that the exact freezing temperature is the mean temperature of the solidification temperature range. For the tuned LTR model to be more flexible in use, it is desired that the resistance tuning curve is independent of boundary conditions and material properties. Ideally, $\partial f_1/\partial \Delta T = 0$ and $\partial f_1/\partial k_{pcm} = 0$. Or at least the effect from those parameters on the accuracy of the tuned LTR model is negligibly small. Nine new cases shown in Table 5 are considered to test the accuracy of the tuned LTR model. The first 3 cases have different side lengths while keeping same driving temperature and PCM conductivity as the cases for building the resistance tuning curve. Cases 4–5 have different driving temperatures. Cases 6 and 7 have different PCM conductivities. Case 8 has both different driving temperature difference and PCM conductivity as the training cases. Case 9 has a much larger driving temperature difference than other cases. Additionally cases 4–9 both have

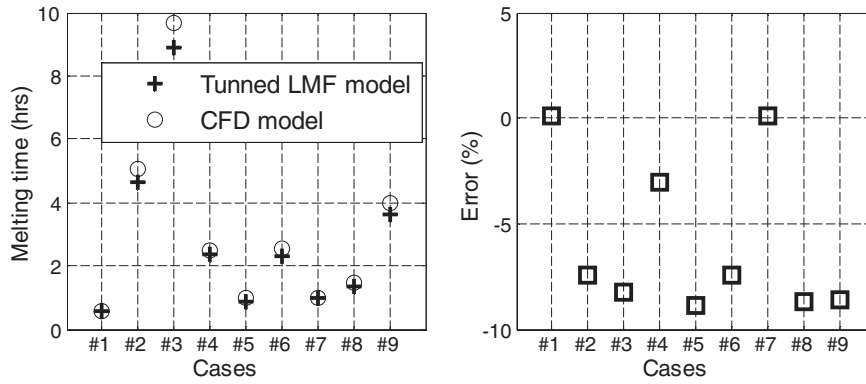


Fig. 6. Predictions of 9 2-D cases using the tuned LTR model.

ter will be defined by a surface $\alpha = f_2(\mu, \gamma)$. To construct this tuning surface in the present example, 4 aspect ratios (0.1, 0.4, 0.7, 1) were assigned to μ, γ . Together there are 16 discrete samples, but due to symmetry, the distinct samples are 10. Table 6 shows specific points that cover the lengths ratios from 0.1 to 1. The Solidification & Melting model [24] In Fluent was used to obtain the numerical results. In the CFD model a solidification temperature range $T_{upper} - T_{lower} = 1^\circ\text{C}$ was set, the initial temperature was T_{upper} everywhere and $T_{upper} - T_w = 10^\circ\text{C}$. Eqs. (2.21)–(2.24) show the thermal resistances calculation procedures of the 3-D tuned LTR model, the heat flux and solidification calculations are same as the Eqs. (2.11)–(2.13) in Section 2.2. Fig. 8 shows the solidification time surfaces of the 16 points estimated by CFD model and the LTR model without a resistance tuning factor. There is obvious deviation in amplitude but the shape of the surfaces by the two models shares similarity. This suggests that a resistance tuning surface can be constructed based on the solidification time ratios of the two models. A custom support vector regression was applied to build the resistance tuning surface. The two aspect ratios that cover the range (0.1, 1) are the input variables and the solidification time ratio t_{CFD}/t_{LTR} between the LTR model without tuning and CFD mode is the output of the SVR model f_2 . As there are 16 discrete points, the data set is much sparse compared with having 10 data points in the one dimensional case. The regression parameter should indeed be optimized for the smallest possible overall predication error [29].

Fig. 9 shows the tuning surface by the custom SVR model. Table 7 lists the 7 testing cases. Results presented in Fig. 10 shows excellent prediction performance for the tuned LTR model in 3-D. The prediction error is within 4%, which is better than the 2-D case. A possible reason is a smaller solidification temperature range is used for the CFD cases. Analysis of around 150 layered solidification fronts were included in the cases considered. It also demonstrates that the resistance tuning surface and predictions are

independent of boundary temperature and the PCM properties. So this tuning surface is applicable to new cuboid shapes and other PCMs.

$$R_1 = \frac{x}{(a-z)(c-y)k_{pcm}} \tag{2.21}$$

$$R_2 = \frac{z}{(a-z)(b-x)k_{pcm}} \tag{2.22}$$

$$R_3 = \frac{z}{(a-z)(b-x)k_{pcm}} \tag{2.23}$$

$$R_t = \alpha \frac{R_1 R_2 R_3}{R_1 + R_2 + R_3} \tag{2.24}$$

3. Coupled PCM with fins by layered thermal resistance model

Many PCM's used for thermal energy storage are very poor thermal conductors thus posing impediments to energy transfer particularly during the energy retrieval (solidification) process. Fins, embedded graphite and other methods were used overcome this obstacle. Application of the tuned LTR model to a PCM domain containing fins would thus be a natural extension of the method. The discharging process is more difficult to complete as it is conduction controlled [23], while the melting process can be much easier to complete due to the solid sinking phenomenon induced by density differences between the solid and liquid PCM phases [30]. Thus an efficient coupled fin-PCM model based on conduction can prove to be critical and beneficial to the optimal design of an energy storage system with PCM. In this section the tuned LTR model is applied for modeling PCM systems that include plate fins. Note that in the following sections, the finned LTR model means the tuned LTR model that is coupled with fins.

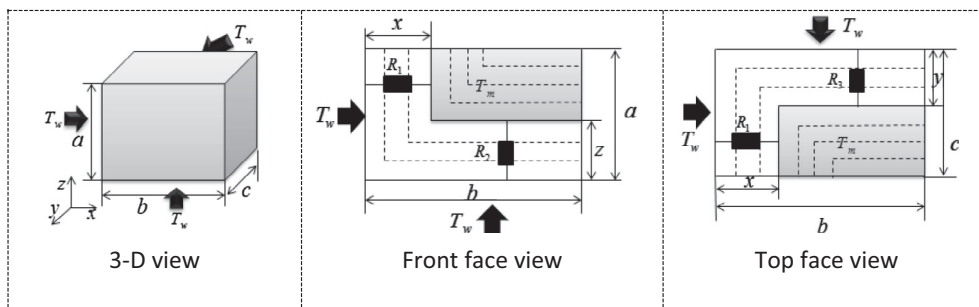


Fig. 7. 3-D cubic PCM cooling from 3 faces with constant temperature.

Table 6
10 Cuboids with different side lengths ratios.

a (cm)	5	5	5	5	5	5	5	5	5
b (cm)	0.5	2	3.5	5	2	3.5	5	3.5	5
c (cm)	0.5	2	3.5	5	0.5	0.5	0.5	2	3.5
b/a	0.1	0.4	0.7	1.0	0.4	0.7	1.0	0.7	1.0
c/a	0.1	0.4	0.7	1.0	0.1	0.1	0.1	0.4	0.7

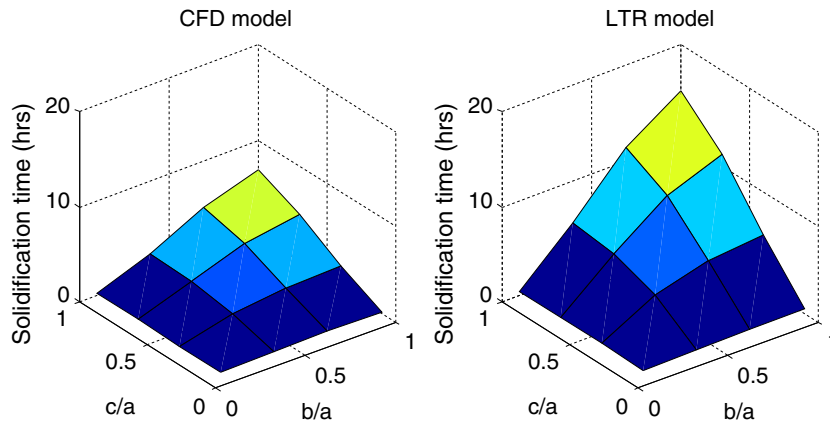


Fig. 8. Solidification time estimation by CFD mode and LTR model without tuning.

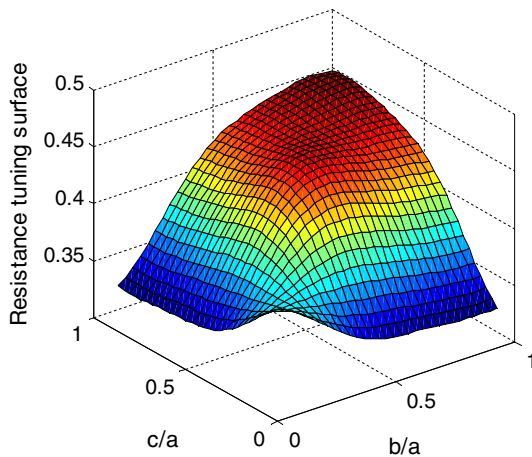


Fig. 9. Resistance tuning surface by support vector regression.

3.1. Coupled PCM fin modeling in 2-D

A rectangular PCM domain with a plate fin on one side as shown in Fig. 11 was studied. The PCM and the fin are cooled at the same end (the edge along the y-axis) with same constant temperature and the other boundaries have zero heat flux. There are two heat paths for energy transfer to the PCM. One path is through PCM with its thermal resistance R_1 and the other one is through the fin, passing through multiple thermal resistances R_{21} , R_{22} , R_{23} . R_1 is the same as Eq. (2.8) in Section 2.2 and R_{23} is a new name to be used in current description but it has the same definition as Eq. (2.9) in Section 2.2. R_{21} and R_{22} are defined as

$$R_{21} = \frac{x}{a\delta k_{fin}} \tag{3.1}$$

$$R_{22} = \frac{\delta}{2a(b-x)k_{fin}} \tag{3.2}$$

where a is the thickness of the rectangular PCM domain and fin in z direction and x is the distance of the solidification front in x direction. R_{21} is the resistance in the fin from the cooling source to the solidification front in x -axis direction. The resistance in the fin for passing the heat from fin to the PCM is R_{22} . This resistance is rather small compared to the others and thus can be neglected. Besides the fin resistances to be incorporated into the tuned LTR model, fin efficiency is also a key factor that must be considered. The fin efficiency (3.3) was derived by solving the energy balance equation of the fin (presented in Appendix A). Thus the thermal resistance passing through the fin needs to be increased by $1/\eta$. Eq. (3.5) is the total resistance for the finned LTR model shown in Fig. 10. The heat flux and solidification time calculations are the same as Eqs. (2.11)–(2.13) listed in Section 2.2.

$$\eta = \frac{T(x) - T_m}{T_w - T_m} = (\cosh(\xi x) - \tanh(\xi b) \sinh(\xi x)) \tag{3.3}$$

$$R_2 = 1/\eta(R_{21} + R_{22}) + R_{23} \tag{3.4}$$

$$R_t = \alpha \frac{R_1 R_2}{R_1 + R_2} \tag{3.5}$$

To test the prediction capabilities of the finned LTR model, 4 different dimensions were considered as shown in Table 8. Three fin thickness (2 mm, 1 mm, 0.5 mm) and two types of fin material

Table 7
New cases for the tuned LTR model testing.

Dimensions (cm)	(2, 2, 2)	(8, 8, 8)	(3, 2, 1)	(7, 4, 2)	(2, 1, 1)	(7, 7, 3)	(9, 8, 7)
ΔT (°C)	10	10	7	20	10	20	15
k_{pcm} (W/(m K))	0.5	0.5	0.5	0.5	0.3	1	3

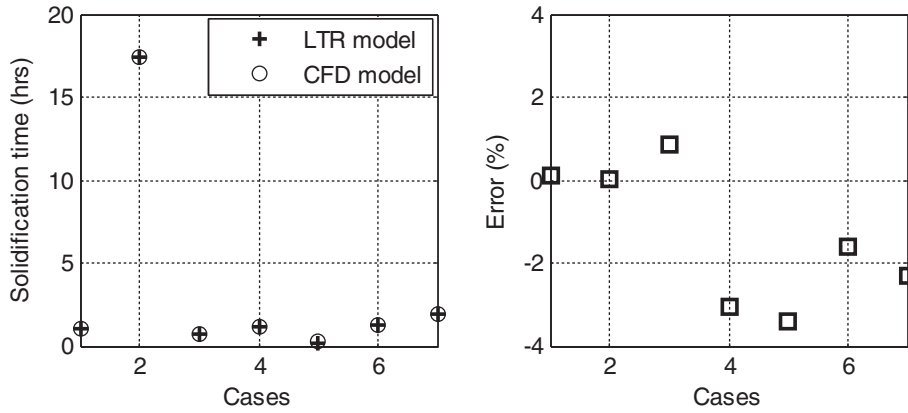


Fig. 10. Predictions of the 7 new cases by the tuned LTR model.

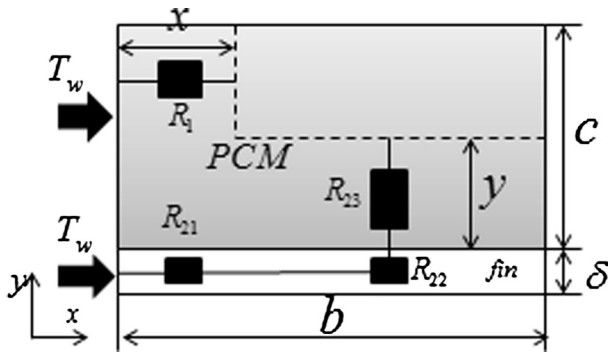


Fig. 11. 2-D coupled PCM fin sketch.

Table 8
New cases for the finned LTR model testing.

Cases	#1	#2	#3	#4
a (cm)	1	1	1	5
b (cm)	1	3	7	5

(aluminum, carbon steel) were also considered, so together there were 24 testing cases. The conductivity of the aluminum fin is 202.4 W/(m K) and that of carbon steel is 50 W/(m K).

Fig. 12 shows the solidification time of all the cases predicted by the finned LTR model (denoted by solid lines) and by CFD model (denoted by circles). Fig. 12 shows the prediction errors as defined in Section 2 Eq. (2.18). From left to right in sequence are the 4 cases; every three points represent the three fin thicknesses (0.5 mm, 1 mm, 2.0 mm). For the aluminum fin cases with different thicknesses, the prediction errors of all the cases are within 4%. For the carbon-steel fin cases, most of them have prediction errors within 5%, except for Case 3 with fin thickness 0.5 mm as shown in Fig. 13. Large prediction error occurs when the fin thickness is small, i.e. 0.5 mm. It is possible that the fin's low efficiency causes the large prediction error, so extra cases were tested to verify this assumption as shown in Tables 9 and 10. In the evaluation of fin efficiency, the heat transfer coefficient is an unknown variable and it is assumed to be the conductivity of PCM divided by the distance from the fin to the solidification front of PCM, $h = k_{pcm}/L$. The distance L in the fin efficiency calculation (Eq. (3.3)) in the finned LTR model changes with the locations of the solidification front and, but here it is set as $L = 1$ cm. The length of the fin, fin thickness and fin material are the dependent variables for the calculation of the fin efficiency. For the aluminum fin in Fig. 14, when the fin

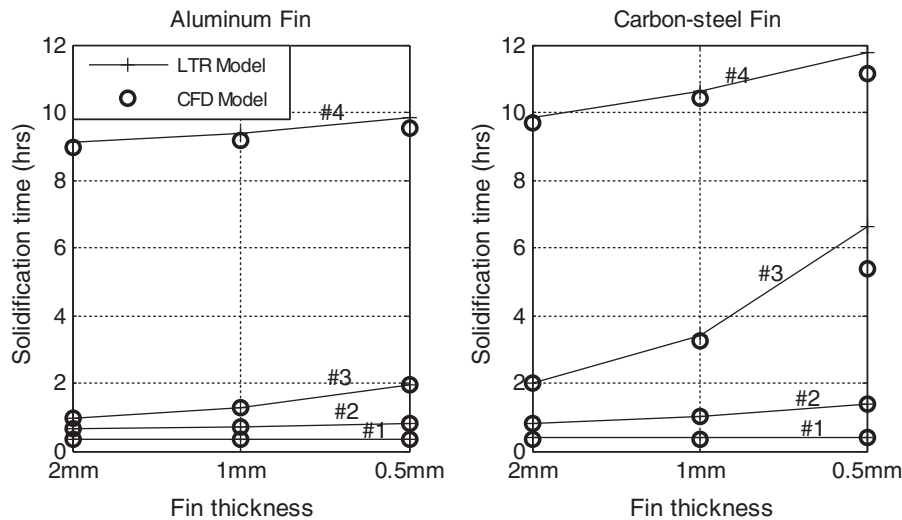


Fig. 12. Predictions of the testing cases by the 2-D Finned LTR model.

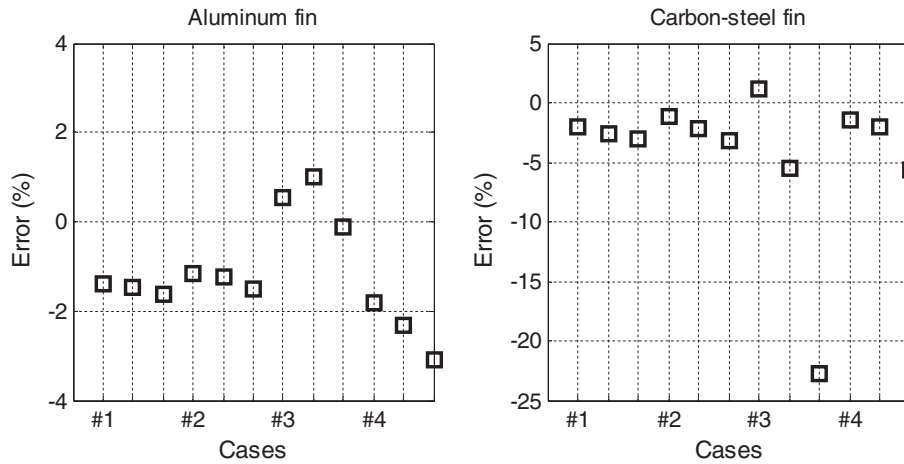


Fig. 13. Predication errors by 2-D Finned LTR model. (Every 3 consecutive points represent fin thickness 0.5 mm, 1.0 mm and 2.0 mm)

Table 9
Extra testing cases for aluminum fin.

Cases	#1	#2	#3	#4
a (cm)	10	10	10	10
b (cm)	150	150	180	210
Fin thickness (mm)	2	1	2	2

Table 10
Extra testing cases for carbon steel fin.

Cases	#1	#2	#3	#4
a (cm)	10	10	10	10
b (cm)	70	70	80	110
Fin thickness (mm)	2	0.5	2	2

efficiency is decreased to 0.2 either due to low fin thickness (comparison between #1 and #2), or the fin is too long (comparison between #3 and #4), the deviation in solidifying time estimation by the finned LTR model becomes large. The same also happens for the carbon-steel fin cases as shown in Fig. 15. Thus it can be concluded that as long as the fin efficiency is not lower than a certain value, the finned LTR model will always give high accurate solidification time estimation.

For modeling PCM only, the heat flux during the solidification process was not considered, but for a finned PCM system it is an important parameter to study the performance of a fin. Fig. 16

shows the solidification fraction curves given by the finned LTR and CFD models and Fig. 17 shows the heat flux curves through the cooling surfaces including both the PCM and fin faces. One case under comparison was Case 1 with 2 mm thick aluminum fin and the other one was Case 4 with 0.5 mm thick carbon-steel fin. Respectively the two cases represent short-time solidification and solidification in a long time period. There is some discrepancy between the two solidification fraction curves predicted by the finned LTR and CFD models. However, the curvature trend for the heat flux matches quite well for both of the two cases. This implies that the finned LTR model also has a good ability to represent the heat flux dynamics during the entire solidification process. Thus the finned LTR model will be a reliable model to be employed in efficient optimal design of a finned PCM system.

3.2. Coupled PCM fin modeling in 3-D

The methods described above can be applied for a more general three dimensional PCM domain with fins. Fig. 18 shows a cuboidal PCM wrapped by three plate fins. The fins were considered to have same thickness. And the system is cooled at the surface of the left plate fin; the remaining faces have zero heat flux. Though conduction paths through the PCM and fins are infinite in nature, it is assumed there are three principal heat paths, each passing through one plate fin and PCM. Based on Fig. 18, the total thermal resistance for the heat path going through the left plate fin is R_{11} and R_{12} is the resistance in

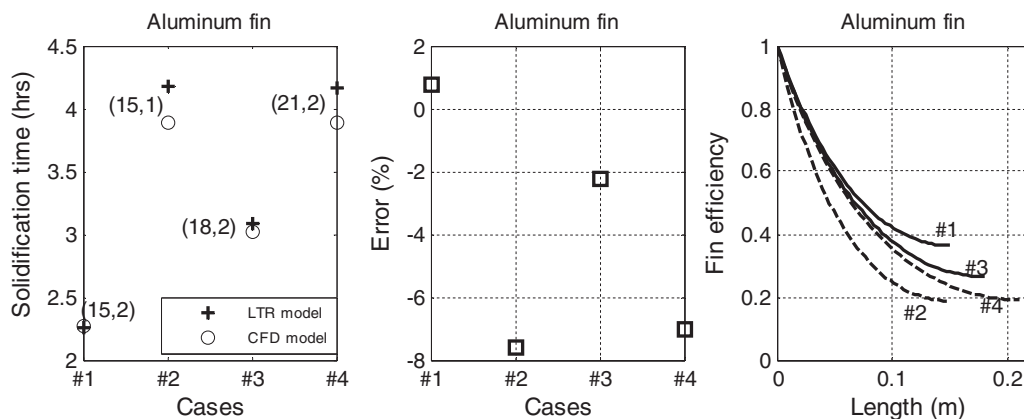


Fig. 14. Solidification time prediction error versus fin efficiency for aluminum fin (in the parentheses (aspect ratio b/c, fin thickness (mm))).

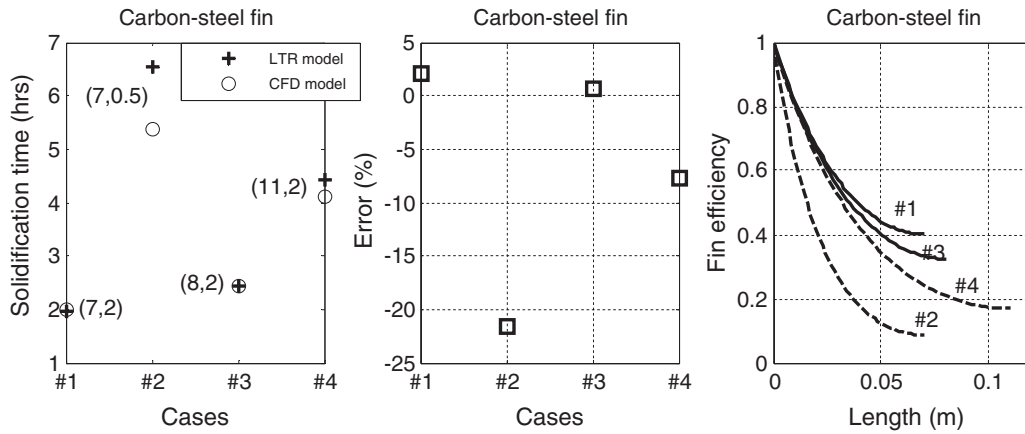


Fig. 15. Solidification time prediction error versus fin efficiency for carbon-steel fin (in the parentheses (aspect ratio b/c, fin thickness (mm))).

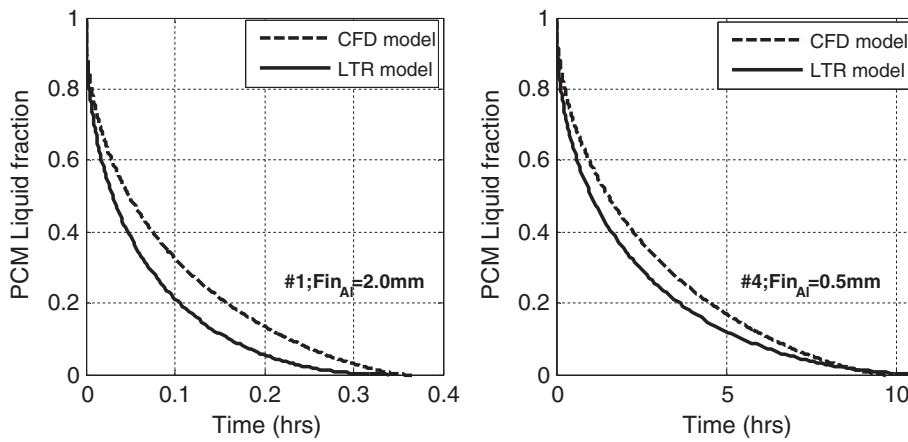


Fig. 16. Solidification fraction curve comparison between the finned LTR and CFD models.

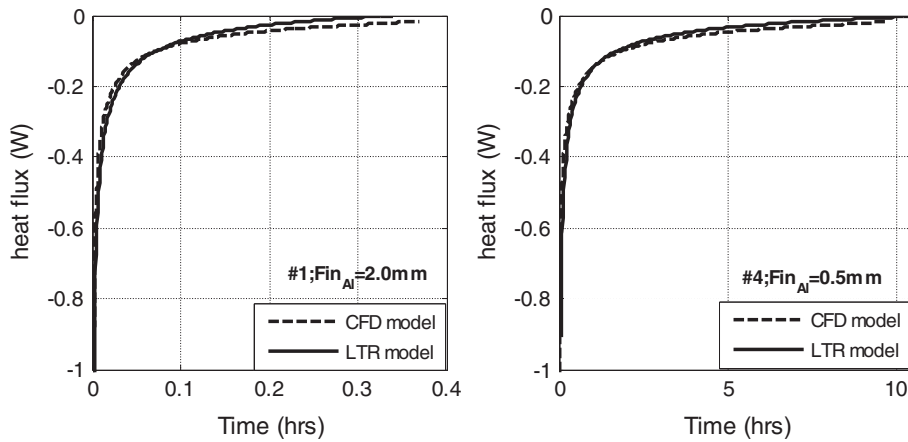


Fig. 17. Heat flux curve comparison between the finned LTR and CFD models.

the PCM for this heat path. The total thermal resistance of the heat path going through the bottom plate fin is R_2 , and R_{21} is the resistance for the heat passing through the fin, R_{22} is the resistance in PCM of this heat path. Similarly R_3 is the total resistance for heat going through the back-plate fin in the figure, its component resistances are R_{31} for the fin and R_{32} for the PCM. It is assumed additionally that heat transfer in the fin only takes place along the

length of the fin (say only along the x direction), so the fin efficiency (3.3) in the 2-D case can also be applied in the plate fins for the 3-D case. Then the heat flux, solidification time calculations are same as those (Eqs. (2.11)–(2.13)) used in the LTR model without fins for the 2-D case. (Note that the names of R_{ij} in Eqs. (3.6)–(3.14) may already appears in the previous sections, but they are redefined under current context.)

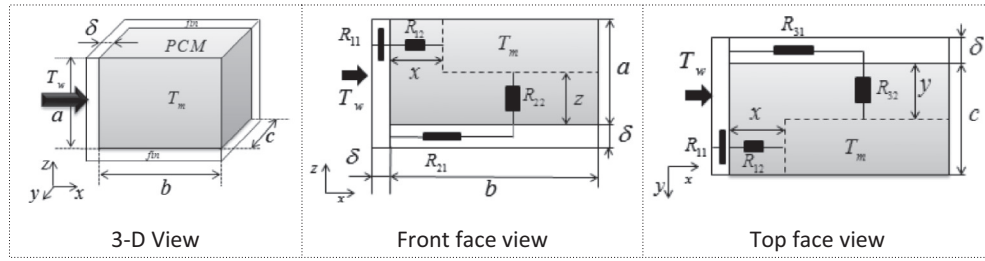


Fig. 18. PCM wrapped in a 3-D plate fins.

Table 11
Test cases for 3-D finned LTR model.

Cases	#1	#2	#3	#4	#5	#6	#7	#8	#9
(a, b, c) (cm)	(2, 2, 2)	(1, 3, 1)	(1, 5, 1)	(1, 7, 1)	(5, 1, 5)	(7, 1, 7)	(6, 6, 6)	(6, 6, 6)	(6, 6, 6)
ΔT ($^{\circ}\text{C}$)	10	10	10	10	10	10	10	20	10
k_{pcm} (W/(m K))	0.5	0.5	0.5	0.5	0.5	0.5	0.5	0.5	1.0

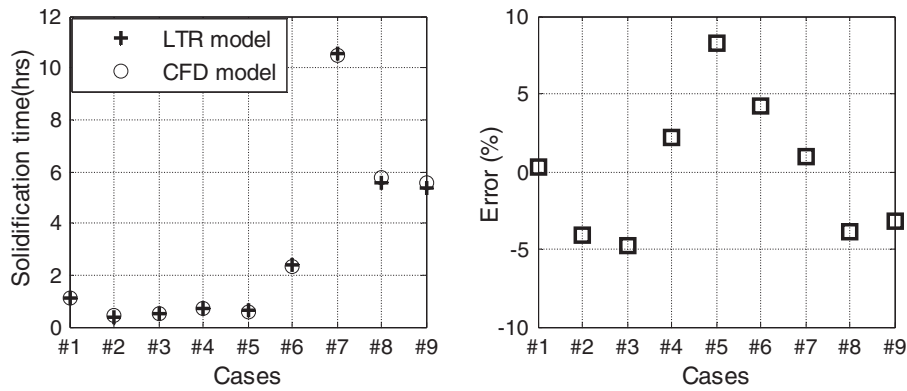


Fig. 19. Solidification time predictions by 3-D finned LTR model.

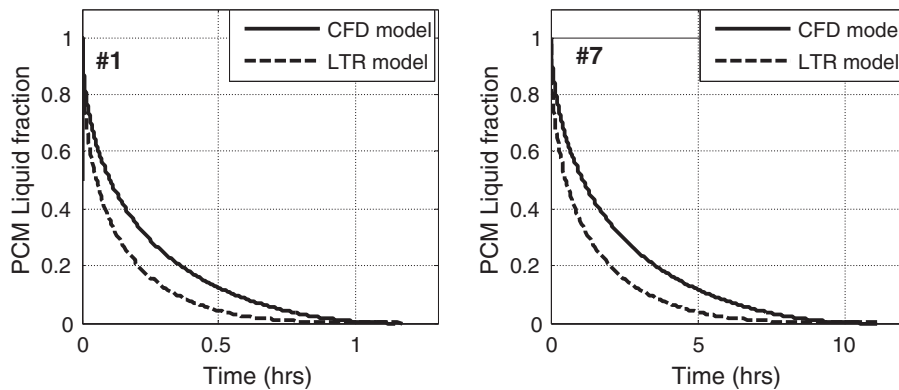


Fig. 20. Solidification fraction curve comparison between finned LTR and CFD models.

$$R_{11} = \frac{\delta}{ca k_{fin}} \quad (3.6)$$

$$R_{12} = \frac{x}{(a-z)(c-y)k_{pcm}} \quad (3.7)$$

$$R_1 = R_{11} + R_{12} \quad (3.8)$$

$$R_{21} = \frac{x}{c\delta k_{fin}} \quad (3.9)$$

$$R_{22} = \frac{z}{(b-x)(c-y)k_{pcm}} \quad (3.10)$$

$$R_2 = \frac{1}{\eta} R_{21} + R_{22} \quad (3.11)$$

$$R_{31} = \frac{x}{a\delta k_{fin}} \quad (3.12)$$

$$R_{32} = \frac{y}{(b-x)(a-z)k_{pcm}} \quad (3.13)$$

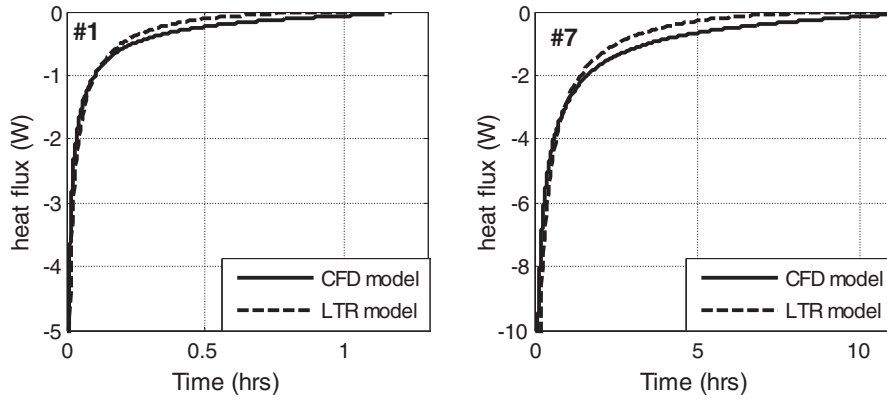


Fig. 21. Heat flux curve comparison between finned LTR and CFD models.

$$R_3 = \frac{1}{\eta} R_{31} + R_{32} \tag{3.14}$$

Nine cases as listed in Table 11 were used to test the performance of the 3-D finned LTR model. The geometries of the testing cases vary from a long bar shape (Case 4) to a plate shape (Case 6). Case 8 considers a different driving temperature difference and Case 9 considers a different PCM conductivity. The fin material is aluminum and its thickness is 1mm. CFD results were obtained by the Solidification & Melting model in Fluent [24]. The solidification time estimation is shown in Fig. 19. Most of the cases have an error within 5%, except for the plate shape case which has an error close to 8%. The performance is not as good as the 2-D situation. The assumption that one-dimensional conduction takes place in the fin is the most possible cause to enlarge the error. The solidification fraction curves and the heat flux curves of Case 1 and Case 7 are shown in Figs. 20 and 21. There are some discrepancy between the two solidification fraction curves predicted by CFD and the finned LTR models. However, the 3-D finned LTR model captures the trend of a heat flux curve very well for both of the cases. The 3-D finned LTR model promises to be an efficient and reliable modeling approach for a finned PCM system considered in Fig. 18 with almost no simulation cost after the tuning surface is built.

4. Conclusion

An efficient method to predict PCM behavior in three dimensions that could include fins is described in this paper. For most of the cases considered here results from the efficient LTR model compare well with those obtained using full scale transient three dimensional CFD methods. The key to successfully building the LTR model is to define the correct ‘tuning curve/surface’ for the geometry and shape of interest. The LTR model described here for Cartesian coordinates can readily be adapted for other complex geometries and coordinates such as cylindrical and/or curvilinear orthogonal coordinates. Then the tuning curve or surface will be dependent on the appropriate chosen ratios of independent parameters. As the finned LTR model represents a PDE described nonlinear transient freezing process into algebraic equations, thus a well-tuned LTR model can become the back-bone of an extensive yet efficient and inexpensive optimal design of a system that uses PCM and fins.

Acknowledgement

This research is sponsored by the ARPA-e ARID Program under Contract No. DE-AR0000582. Any opinions, findings, and conclusions or recommendations expressed in this article are those of

the authors and do not necessarily reflect the views of the Advanced Research Projects Agency-Energy.

Conflict of interest

The authors declared that there is no conflict of interest.

Appendix A

A.1. Fin efficiency calculation

The fin extended from the heat pipe is approximated by a 1D conduction bar. As shown in Fig. A1, it has a constant temperature at one end and heat flux boundary condition on the PCM side; the other end and side have zero heat flux. Based on an energy balance of the bar, the fin efficiency is:

$$\begin{aligned} Q_x &= Q_{x+\Delta x} + Q_c, \quad \Delta x \rightarrow 0 \Rightarrow Q_{x+\Delta x} \\ &= Q_x + \frac{dQ_x}{dx} \Delta x, \quad \frac{dQ_x}{dx} \Delta x + Q_c = 0 \end{aligned} \tag{A.1}$$

$$Q_x = -k_{fin} A \frac{dT}{dx}, \quad Q_c = hS(T - T_{pcm}) \tag{A.2}$$

$$A = cw, \quad S = c\Delta x, \quad h = \frac{k_{pcm}}{L} \quad (c: \text{Thickness of the fin}) \tag{A.3}$$

$$\frac{d}{dx} \left(-k_{fin} A \frac{dT}{dx} \right) + hS(T - T_{pcm}) = 0, \quad \text{assuming } \theta = T(x) - T_{pcm} \tag{A.4}$$

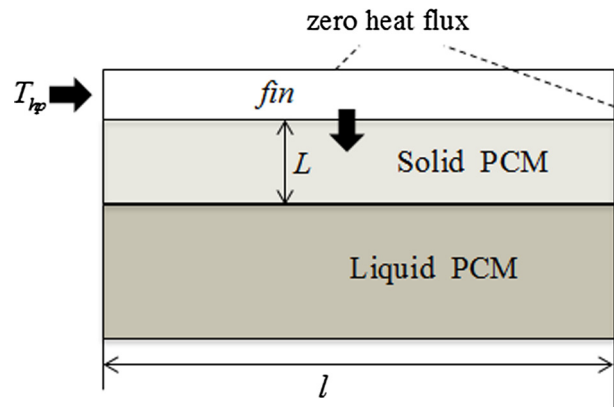


Fig. A1. Geometry and boundary conditions for the 1-D bar efficiency calculation.

$$\frac{d^2\theta}{dx^2} - \frac{k_{pcm}}{k_{fin}wL} \theta = 0, \quad \theta|_{x=0} = T_{hp} - T_{pcm}, \quad \left. \frac{\partial\theta}{\partial x} \right|_{x=L} = 0 \quad (\text{A.5})$$

$$\xi^2 = \frac{k_{pcm}}{k_{fin}wL}, \quad (\text{A.6})$$

$$\theta = (T_{hp} - T_m) (\cosh(\xi x) - \tanh(\xi l) \sinh(\xi x)) \quad (\text{A.7})$$

$$\eta = \frac{T(x) - T_m}{T_w - T_m} = (\cosh(\xi x) - \tanh(\xi l) \sinh(\xi x)) \quad (\text{A.8})$$

where L is the melting front distance away from the fin. The heat transfer coefficient at the PCM side is assumed to be the conductivity of the PCM divided by the melting front distance, $h = k_{pcm}/L$.

References

- [1] Mohammad Hoseini Rahdar, Abolghasem Emamzadeh, Abtin Ataei, A comparative study on PCM and ice thermal energy storage tank for air-conditioning systems in office buildings, *Appl. Therm. Eng.* 96 (2016) 391–399.
- [2] Nasiru I. Ibrahim et al., Experimental testing of the performance of a solar absorption cooling system assisted with ice-storage for an office space, *Energy Convers. Manage.* 148 (2017) 1399–1408.
- [3] F. Agyenim, N. Hewitt, P. Eames, et al., A review of materials, heat transfer and phase change problem formulation for latent heat thermal energy storage systems (LHTESS), *Renew. Sustainable Energy Rev.* 14 (2010) 615–628.
- [4] M.K. Rathod, J. Banerjee, Thermal stability of phase change materials used in latent heat energy storage systems: a review, *Renew. Sustain. Energy Rev.* 18 (2013) 246–258.
- [5] E. Fleming, S. Wen, L. Shi, et al., Experimental and theoretical analysis of an aluminum foam enhanced phase change thermal storage unit, *Int. J. Heat Mass Transf.* 82 (2015) 273–281.
- [6] J.M. Khodadadi, S.F. Hosseinizadeh, Nanoparticle-enhanced phase change materials (NEPCM) with great potential for improved thermal energy storage, *Int. Commun. Heat Mass* (34) (2007) 534–543.
- [7] A. Jamekhorshid, S.M. Sadrameli, M. Farid, A review of microencapsulation methods of phase change materials (PCMs) as a thermal energy storage (TES) medium, *Renew. Sustain. Energy Rev.* 31 (2014) 531–542.
- [8] S. Lohrasbi, M. Sheikholeslami, D.D. Ganji, Discharging process expedition of NEPCM in fin-assisted latent heat thermal energy storage system, *J. Mol. Liq.* 221 (2016) 833–841.
- [9] S. Lohrasbi, S.Z. Miry, M. Gorji-Bandpy, et al., Performance enhancement of finned heat pipe assisted latent heat thermal energy storage system in the presence of nano-enhanced H_2O as phase change material, *Int. J. Hydrogen Energy* 42 (2017) 6526–6546.
- [10] Peleg P. Levin, Avraham Schitzer, Ga.d. Hetsroni, Numerical optimization of a PCM-based heat sink with internal fins, *Int. J. Heat Mass Transfer* 61 (2013) 638–645.
- [11] Manish K. Rathod, Jyotirmay Banerjee, Thermal performance enhancement of shell and tube latent heat storage unit using longitudinal fins, *Appl. Therm. Eng.* 75 (2015) 1084–1092.
- [12] Zhuo Li, Wu. Zhi-Gen, Analysis of HTFs, PCMs and fins effects on the thermal performance of shell-tube thermal energy storage units, *Sol. Energy* 122 (2015) 382–395.
- [13] M. Sheikholeslami, S. Lohrasbi, D.D. Ganji, Response surface method optimization of innovative fin structure for expediting discharging process in latent heat thermal energy storage system containing nano-enhanced phase change material, *J. Taiwan Inst. Chem. Eng.* 67 (2016) 115–125.
- [14] M. Sheikholeslami, S. Lohrasbi, D.D. Ganji, Numerical analysis of discharging process acceleration in LHTESS by immersing innovative fin configuration using finite element method, *Appl. Therm. Eng.* 107 (2016) 154–166.
- [15] S. Lohrasbi, M. Sheikholeslami, D.D. Ganji, Multi-objective RSM optimization of fin assisted latent heat thermal energy storage system based on solidification process of phase change Material in presence of copper nanoparticles, *Appl. Therm. Eng.* 118 (2017) 430–447.
- [16] S.J. Ren, J. Charles, X.C. Wang, et al., Corrosion testing of metals in contact with calcium chloride hexahydrate used for thermal energy storage, *Mater. Corros.* 10.1002/maco.201709432.
- [17] Hu Henry, Stavros A. Argyropoulos, Mathematical modelling of solidification and solidifying: a review, *Model. Simul. Mater. Sci. Eng.* 4 (1996) 371–396.
- [18] J. Stefan, S.B. Wien, *Akad. Mater. Nature* 98 (473–484) (1889) 965–983.
- [19] P. Lamberg, K. Siren, Analytical model for solidification in a semi-infinite PCM storage with an internal fin, *Heat Mass Transf.* 39 (2003) 167–176.
- [20] P. Lamberg, K. Siren, Approximate analytical model for solidification in a finite PCM storage with internal fins, *Appl. Math Model* 27 (7) (2003) 491–513.
- [21] P. Lamberg, Approximate analytical model for two-phase solidification problem in a finned phase change material storage, *Appl. Energy* 77 (2) (2004) 131–152.
- [22] Parham A. Mirzaei, Fariborz Haghghat, Modeling of phase change materials for applications in whole building simulation, *Renew. Sustain. Energy Rev.* 16 (2012) 5353–5362.
- [23] S. Jegadheeswaran, S.D. Pohekar, Performance enhancement in latent heat thermal storage system: a review, *Renew. Sustain. Energy Rev.* 13 (9) (2009) 2225–2244.
- [24] <https://www.sharcnet.ca/Software/Fluent6/html/ug/node973.htm>.
- [25] A.D. Brent, V.R. Voller, K.J. Reid, Enthalpy-porosity technique for modeling convection-diffusion phase change: application to the solidifying of a pure metal, *Num. Heat Transf. Part A* (13) (1988) 297–318.
- [26] K.A.R. Ismail, C.L.F. Alves, M.S. Modesto, Numerical and experimental study on the solidification of PCM around a vertical axially finned isothermal cylinder, *Appl. Therm. Eng.* 21 (2001) 53–77.
- [27] <https://www.mathworks.com/help/stats/support-vector-machine-regression.htm>.
- [28] https://en.wikipedia.org/wiki/Spline_interpolation.
- [29] A.J. Smola, B. Schölkopf, A tutorial on support vector regression, *Stat. Comput.* 14 (2004) 199–222.
- [30] Y. Kozak, T. Rozenfeld, G. Ziskind, Close-contact melting in vertical annular enclosures with a non-isothermal base: theoretical modeling and application to thermal storage, *Int. J. Heat Mass Transf.* 72 (2014) 114–127.